Petroleum Science 18 (2021) 1033–1046

Contents lists available at ScienceDirect

Petroleum Science

journal homepage: www.keaipublishing.com/en/journals/petroleum-science

Original Paper

Source and accumulation process of Jurassic biodegraded oil in the Eastern Junggar Basin, NW China

Mao-Guo Hou [a], Ming Zha [a], Xiu-Jian Ding [a, *], He Yin [b], Bao-Li Bian [b], Hai-Lei Liu [b], Zhong-Fa Jiang [b]

[a] School of Geosciences, China University of Petroleum, Qingdao, Shandong 266580, China
[b] Research Institute of Exploration and Development, Xinjiang Petroleum Administration Bureau, Karamay 834000, China

ARTICLE INFO

Article history:
Received 17 April 2020
Accepted 10 December 2020
Available online 12 July 2021

Edited by Jie Hao

Keywords:
Biodegraded oil
Mixed oil
Oil-source correlation
Oil accumulation process
Junggar Basin

ABSTRACT

Biodegradation usually obscures or even radically alters the original characteristics of oil biomarkers. The mixing of oil from multiple sources makes each source difficult to trace. Identifying the source of biodegraded oil from multiple sources has always been a hard nut to crack. Rising to this challenge, in this study-we carried out a comprehensive investigation of biodegradation impacts, oil-source correlation, and oil charging history to trace the source and reveal the mixing process of biodegraded oil in the Toutunhe Formation (J_2t) in the eastern Junggar Basin, NW China. The oil of this area was biodegraded to different extent, consequently, many commonly used biomarker parameters (e.g. Pr/Ph, Pr/nC_{17}) became less powerful for oil-source correlation. To address this problem, the resistance of many biomarkers to biodegradation was analyzed, and those of high bio resistance were selected to generate a more reliable oil-source correlation. The results revealed that biodegraded oil was a mixture of oil sourced from Lucaogou Formation (P_2l) and Xiaoquangou Formation ($T_{2\text{-}3}xq$). Core sample observation, microscopic fluorescent analysis and fluid inclusion analysis were combined to analyze comprehensively oil charging history. The analysis of accumulation process exhibited that the existing oil in J_2t was a mixture originated from the P_2l and $T_{2\text{-}3}xq$ source rocks in two separate charging stages when it underwent a complicated process of charging, biodegradation, recharging and mixing.

1. Introduction

Biodegradation is one of the most common secondary alteration effects of oil reservoirs, bringing about the overwhelming majority of heavy oils worldwide (Head et al., 2003; Larter et al. 2003, 2006). Biodegradation acts to break down hydrocarbons, leaving the residual oil enriched in polar molecules and asphaltene fractions. As a result, biodegraded oil is typical of high density and viscosity with high contents of sulfur, resins, asphaltenes, and metals (e.g. Ni and V) (Larter et al., 2003; Pan et al., 2007; Bao et al., 2007; Bao and Zhu, 2009). Moreover, biomarkers that are more susceptible to biodegradation tend to be degraded faster, therefore, these biomarkers or biomarker parameters (e.g. phytane, nC_{25}, C_{30}hopane, phytane/n-octadecane) appear in good correlations with burial depth as published in many investigations (Larter et al. 2003, 2006, 2006; Bennett et al., 2013). The intensity of biodegradation of organic molecules depends not only on the habitual nature of microorganisms, but also on the structures of organic molecules. Typically, structurally simple organic compounds are preferentially degraded than complex ones. For example, isoalkanes are degraded prior to naphthenes but after *n*-alkanes, that is to say, organic compounds with low carbon number are typically consumed prior to those with high carbon number (Schaefer and Leythaeuser, 1980; Peters et al., 2005). Biomarkers carry a record of the source of organic matter, thermal maturation, and depositional environment (Abbott et al., 1985; Chen et al., 1996; Peters et al., 2005; Hao et al., 2011; Wang et al., 2017), therefore, the oil-source correlation study by using source-related biomarkers could, in theory, be an effective method to identify the source of crude oil (Peters et al., 2005; Hao et al., 2011). However, the biodegradation process usually masks the original characteristics of biomarkers, which makes them less powerful to correlate biodegrade oil and source (Bao et al., 2007; Dawson et al., 2013). So, identifying the source of biodegraded oil

* Corresponding author.
E-mail address: dingxj@upc.edu.cn (X.-J. Ding).

https://doi.org/10.1016/j.petsci.2021.07.010

has always been a challenge for researchers worldwide.

Subsurface accumulations of biodegraded oil are common worldwide, such as the Orinoco heavy oil in Venezuela (Mu et al., 2009), the Athabasca oil sands in the Western Canada Basin (Zhou et al., 2008; Hubert et al., 2012), aside from the biodegraded oil reservoirs in the Junggar Basin (Zhang et al., 1988; Chen et al. 2003, 2014; Lu et al., 2016; Huang and Li, 2017), Tarim Basin (Zhang et al., 2014), Bohai Bay Basin (Cheng et al., 2018), and Liaohe Basin (Huang and Larter, 2014) of China. Moreover, the Carboniferous (Chang et al., 2018), Triassic and Cretaceous systems (Zhang et al., 1988; Huang and Li, 2017) in the western Junggar Basin and the Triassic and Jurassic systems (Chen et al. 2003, 2014; Lu et al., 2016) in the eastern Junggar Basin have, thus far, produced a considerable amount of biodegraded oil. The Jurassic, our target system and home to biodegraded oil, is one of most petroliferous systems in the eastern Junggar Basin. Many investigators (Chen et al. 2003, 2014; Lu et al., 2015; Zou et al., 2017) have discussed the source of Jurassic crude oil. Unfortunately, they may fail to point out the impact of biodegradation in their oil-source correlation investigations (Chen et al. 2003, 2014; Zou et al., 2017). And biomarkers (e.g. pristane, phytane, and normal alkanes) that are susceptible to biodegradation are used for oil-source correlation, which could possibly lead to some misleading conclusions. A more accurate approach of tracing oil source shall not only analyze the affinity of biomarkers, but also involve the geological reality of reasonable history match with oil generation and oil charging, yet the latter is what may be neglected in many previous investigations. In this paper, we analyzed the effect of biodegradation on oil and further selected more reliable biomarker parameters affected less by biodegradation to trace oil source. In addition, oil accumulation process was investigated to match the results of oil-source correlation with the geological reality. The results of this study could play an important role in guiding future exploration in the eastern Junggar Basin, as well as provide a more valuable approach to identify the source of biodegraded oils in other similar areas.

2. Geological setting

The Junggar Basin, located in the northwest of China (Fig. 1a), is the second largest sedimentary basin and one of most petroliferous basins in China. The study area, lies in the eastern Junggar Basin (Fig. 1b), covering the eastern part of Fukang Sag and Beisantai Uplift with an area of approximately 2,325 km^2 (Fig. 1b). The basement of the eastern Junggar Basin is a Carboniferous basement, and its sedimentary units ranges from Permian to Quaternary (Fig. 1b). Multistage tectonic movements of Hercynian, Indosinian, Yanshanian, and Himalayan (Zhang et al., 2001; Ding et al., 2017) caused frequent uplifts and subsidences of strata, resulting in a large number of West-East faults (Wu et al., 2014; Chen et al., 2016) and unconformities (Wu et al., 2002; He, 2007).

Our study target, the Toutunhe Formation (J_2t) t in the Middle Juraasic System of the eastern Junggar Basin, is one of most petroliferous systems with great proven oil reserves and undiscovered resources. The sedimentary facies of J_2t is characterized by meandering river delta (Zhang et al., 2001; Bao et al., 2002a,b). The dominant lithology of lower member of J_2t is greyish-green or gray medium-fine grained sandstone, while upper member is dominated by greyish-green mudstone (Fig. 1c). The sandstones in the lower member of J_2t are superior reservoirs with porosity ranging from 5.4% to 31.67% and an average of 16.89%, which are well sealed by mudstones in the upper member of J_2t and the Lower Qigu Formation (J_3q). Oil and gas exploration of the Jurassic System began and expanded in the last decade, during which Santai and Fudong oilfields that contained several lithological oil reservoirs were discovered (Chen et al. 2003, 2014). The Well F32 drilled in 2018 discovered significant hydrocarbon reserves, and produced at 166 t/d of oil and 20,610 m^3/d of gas, which indicated high exploration potential of the Jurassic System with estimated oil reserve of 8.242×10^7 t (Chen et al., 2014).

3. Samples and methods

3.1. Sample information

A total of 306 samples, including source rocks from the P_2l, the $T_{2\text{-}3}xq$, and the Jurassic; free oils and oil-bearing sandstone samples, were studied. 71 source rock samples were used for total organic carbon (TOC) and Rock–Eval analysis. 70 source rock samples and 44 oil-bearing sandstone samples were selected for compound-specific stable carbon isotope analyses. 48 source rock samples and 68 free oil or sandstone samples were used for GC and GC–MS analyses. Fluid inclusion observation and measurement was conducted on 5 reservoir rock samples.

3.2. TOC and Rock-Eval analysis

The TOC of the core samples was measured using a LECO CS-230 analyzer. A Rock–Eval instrument was used to measure S_1, S_2 and T_{max} (temperature of maximum kerogen cracking) following the analysis method of Chinese Petroleum Industry Standard of Rock-Eval analysis GB/T 18602-2012. The temperature was set at 300 °C and held for 3 min, and then turned up to 650 °C at a rate of 25 °C/min.

3.3. Carbon isotope analysis

70 source rock samples and 44 oil-bearing sandstone samples were selected for stable carbon isotope analysis. The source rock and oil-bearing sandstone samples were crushed to 80 mesh. 30 g of crushed samples were extracted by chloroform following Soxhlet method for 72 h to obtain chloroform extracts. The carbon isotope analysis for extracts were carried on a FLASH HT EA-MAT 253 IRMS. Test conditions were as follow: helium (99.999%) as carrier gas with flow 100 mL/min flowrate, oxygen (99.995%) as combustion gas with 250 mL/min flowrate, 980 °C reactor Temperature, reactor filling materials of chromium oxide, reduced copper, and silver/cobalt oxide. Results were reported in standard per mil δ-notation relative to the V-PDB standard.

3.4. GC and GC–MS analysis

The gas chromatograph (GC) used for analyzing the saturated fractions was a Hewlett-Packard 6890 fitted with an HP-5 column (30 m × 0.32 mm × 0.25 μm). Nitrogen was used as carrier gas. The GC oven temperature was initially set at 80 °C for 5 min, then programmed to 290 °C at 4 °C/min and held for 30 min. The gas chromatography–mass spectrometry (GC–MS) analysis of saturated hydrocarbon was performed using a Thermo-Trace GC Ultra-DSQ II system, equipped with an HP-5MS fused silica column (60 m × 0.25 mm × 0.25 μm). Helium was used as carrier gas, with a pilot pressure of 30 psi. The GC oven was initially set at 100 °C and held for 5 min, and subsequently increased to 220 °C at 4 °C/min, and eventually to 320 °C at 2 °C/min. The temperature was held at 320 °C for 20 min. The transfer line temperature was set at 280 °C and the ion source temperature at 280 °C. The GC–MS system was operated in the electron impact (EI) mode with 70 eV and 200 mA. Following the same testing procedures, a total of 116 samples were analyzed, which includes source rocks of P_2l and $T_{2\text{-}3}xq$, and free oils and oil-bearing sandstones from the Fudong and Santai

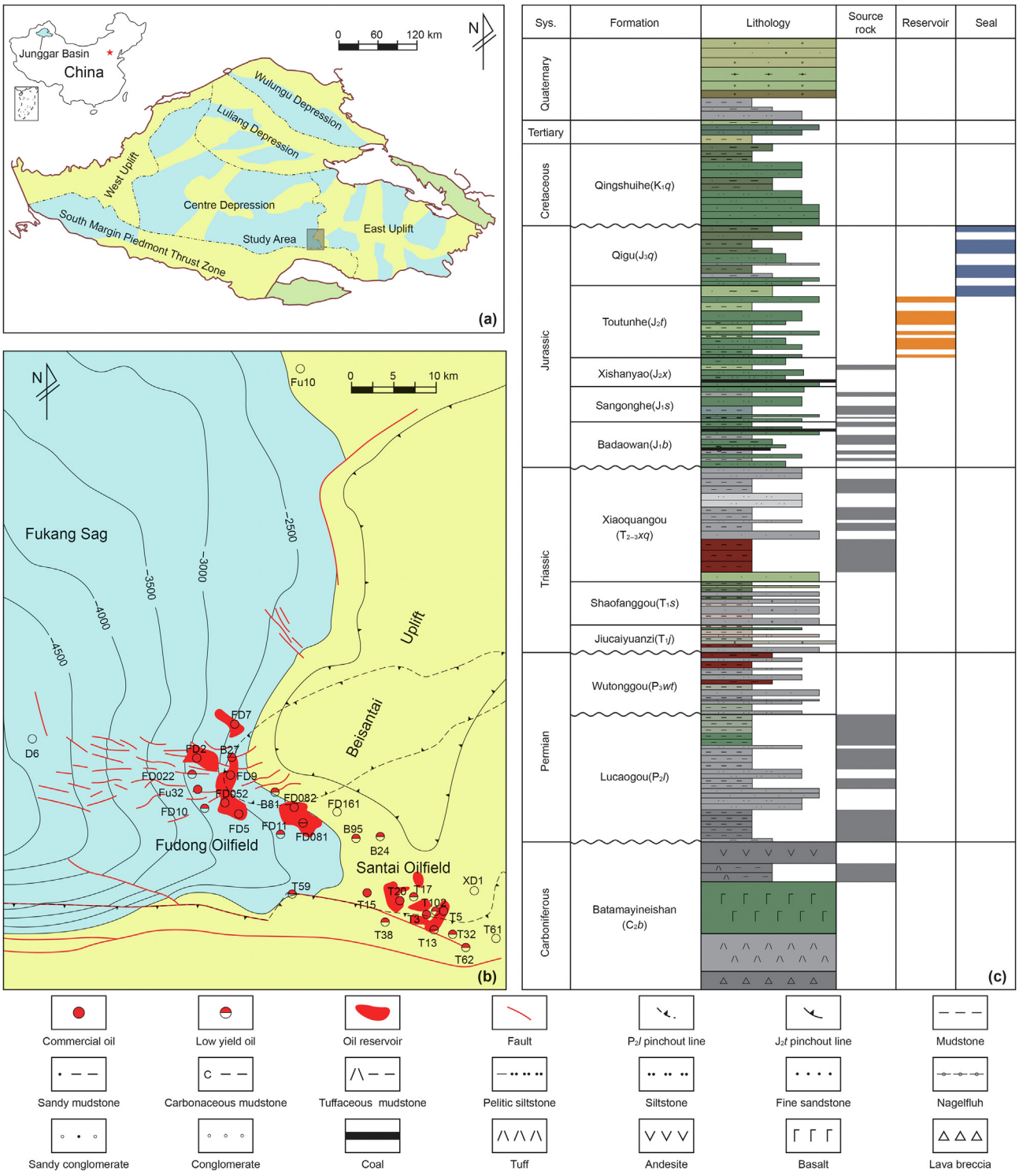

Fig. 1. (a) Map of the Junggar Basin in northwestern China, showing the location of the study area; (b) structure-contour map of the surface of the Toutunhe Formation in the eastern Junggar Basin; (c) summary lithostratigraphy of the eastern Junggar Basin, showing potential source rocks, reservoirs, and seals. Sys. = System.

oilfields.

3.5. Microthermometry of fluid inclusions

Polished thin sections were prepared for fluid inclusion observation and then measured under a Leica DMRXP optical microscope, following the method of Chinese Petroleum Industry Standard SY/T6010-2011. Microthermometry was conducted on a Linkham THMSG600 heating–cooling stage. The fluid inclusion test involved two steps. The first step was to observe the diagenetic process of hydrocarbon-bearing inclusions in thin sections. The second step was to measure the homogenization temperature of the brine inclusions associated with hydrocarbon–bearing inclusions. All of the above instrumentation and processing

procedures were accredited by the China Metrology Accreditation (CMA). Because Since the presence of oil inclusions tends to provide poor estimates of their trapping temperature, homogenization temperatures were only measured on the primary homogeneous phase brine inclusions that are paragenetic with oil inclusions (Emery and Robinson, 1993). For two-phase (liquid and vapor) aqueous inclusions in oil-bearing sandstone samples, measurements of the homogenization temperatures were taken on double-side polished wafers. The heating and cooling rates were 5 °C/min and the accuracy of the homogenization temperature was about 0.1 °C. A total of 37 fluid inclusions from 5 core samples were investigated.

3.6. Basin modelling

Basin modelling is a widely used technique to reconstruct the burial and thermal histories. Its applications have been successful in many petroliferous basins at various locations (Shalaby et al. 2011, 2013; Hakimi and Abdullah 2015a, 2015b; Ding et al., 2018). In this study, we used the BasinMode Software to simulate the thermal and hydrocarbon generation histories of P_2l, $T_{2\text{-}3}xq$, and Jurassic source rocks. Based on this, the burial and thermal histories of the region were reconstructed through one-dimensional modelling of Well Fu10 and B81. The geological data inputs in the simulation were the present-day thicknesses, lithologies, depths, and temperatures of the strata, and the input geochemical parameters included TOC, R_o and Rock-Eval pyrolysis data. Maturity was calculated using the Easy% R_o model of Sweeney and Burnham (1990).

4. Results and discussion

4.1. Biodegradation and its impact

4.1.1. Physical properties and bulk composition

The physical properties and bulk composition of oil are good indicators of biodegradation (Moldowan and Talyzina, 1998; Larter et al., 2003; Peters et al., 2005). The density of crude oil from Santai and Fudong oilfields was positively correlated with viscosity (Fig. 2). The density of oil (test temperature 20 °C) from Fudong Oilfield ranged from 0.8205 to 0.9342 g/cm^3 with an average of 0.8631 g/cm^3, indicating that crude oil was light (0.805–0.870 g/cm^3) or intermediate (0.870–0.934 g/cm^3) oil. The viscosity of crude oil (test temperature 50 °C) from Fudong Oilfield display an extentsive range from 1.0 to 1,000 mPa s. In contrast, the oil of Santai Oilfield was heavier as its densities were mostly over 0.880 g/cm^3 showing an average value of 0.9175 g/cm^3. The viscosity values were above 100 mPa s with the maximum up to 118,000 mPa s.

The analysis on the bulk composition of oil suggested strongly that the content of saturated hydrocarbon was negatively correlated with density (Fig. 3). This was due to the priority degradation of saturated hydrocarbon compared to aromatic hydrocarbon, non-hydrocarbon & asphaltene. The distribution of saturated hydrocarbon content of crude oil from Fudong oilfield was relatively discrete. The majority of saturated hydrocarbon content of light, intermediate, and heavy oils was >65%, 55%–65%, and <45%, respectively. In contrast, oils from Santai Oilfield had lower saturated hydrocarbon content, higher non-hydrocarbon & asphaltene contents than those from Fudong Oilfield. To be more specific, the saturated hydrocarbon content of intermediate oil from two oilfields was similar, while heavy oil form Santai Oilfield had lower saturated hydrocarbon content (35%–50%) relative to Fudong oilfield. Biodegradation could explain this difference, in other words, oils from Santai Oilfield had been more severely biodegraded than those from Fudong Oilfield. This is supported by the theory that non-hydrocarbon & asphaltene are considered to be more resistant to biodegradation than saturated hydrocarbon (Peters et al., 2005).

4.1.2. GC and GC-MS

Due to different resistance to biodegradation, organic molecules tend to be degraded at different rates (Larter et al., 2003; Peters et al., 2005; Bennett et al., 2013; Wang et al., 2013). The first indications of oil biodegradation typically occurred with the selective removal of normal alkanes. As biodegradation proceeded, normal alkanes are degraded faster than mono- and multi-methylated alkanes (Peters et al., 2005). When oil was very slightly or slightly biodegraded as shown in Well FD022 and FD7, almost all the normal alkanes were readily detected on the TIC (total ion chromatogram) gas chromatogram (Fig. 4a, **b**). Further onto moderate

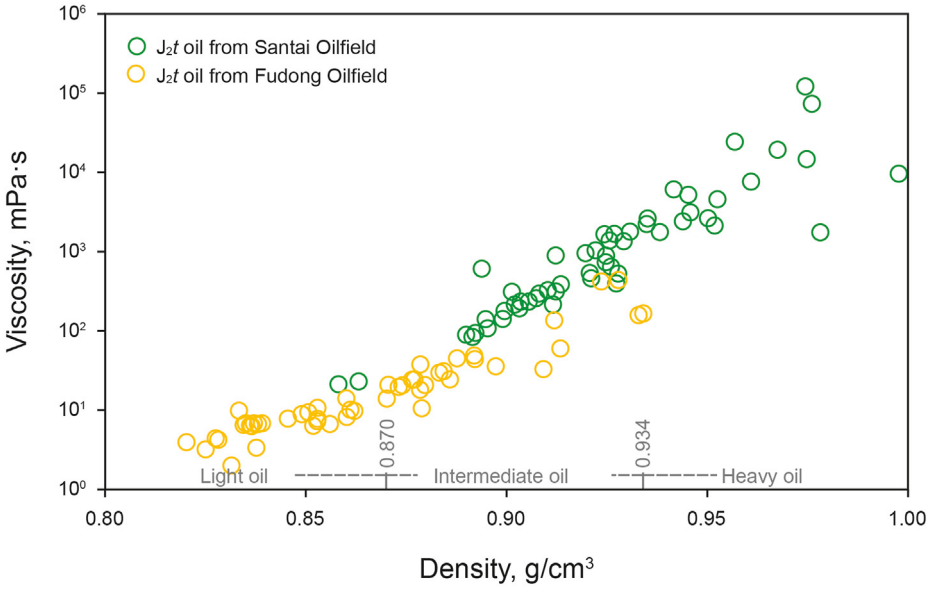

Fig. 2. Density versus viscosity of oil from Santai and Fudong oilfields.

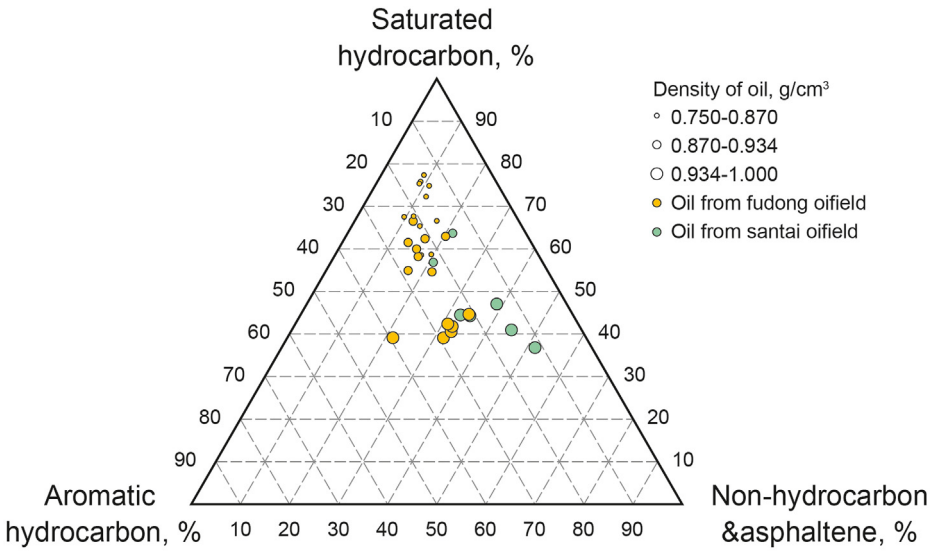

Fig. 3. Ternary plot showing relative abundances of saturated hydrocarbon, aromatic hydrocarbon and non-hydrocarbon & asphaltene.

biodegradation, normal alkanes were obviously consumed (Fig. 4c). When it comes to heavy biodegradation, vast majority of the normal alkanes were significantly consumed (Fig. 4d). When the normal alkanes were almost broken down entirely, the major resolved compounds diminished, and the chromatographic baseline hump became more prominent, reflecting the presence of considerable unresolved complex mixture (UCM). Normal and branched alkanes had the highest susceptibility to biodegradation, followed by acyclic isoprenoids such as pristane and phytane (Peters et al., 2005). When oil samples were very slightly or slightly biodegraded, nC_{17} and nC_{18} exhibited significantly higher abundances than pristane and phytane (Fig. 4a, b). As biodegradation proceeded, the difference virtually disappeared as shown in Fig. 4c to f. In the case of heavy biodegradation, pristane and phytane were also largely removed, subsequently, the absolute abundances of them were significantly lower (Fig. 4d).

Many biodegraded oils contained abundant 25-norhopanes (Trendel et al., 1990; Li et al., 2015), and high abundance of 25-norhopanes was the evidence for heavy or severe biodegradation. Among all oil samples, 25-norhopanes were only detected in a small number of samples. These oil samples detected 25-norhopanes were heavily biodegraded, the majority of them were distributed in Santai Oilfield, and the buried depth was generally less than 2300m. On the m/z 177 mass chromatogram, the 25-norhopanes with carbon number of 28–31 were only detected in heavily biodegraded oils (Fig. 4h), whereas they were absent in the very slightly, slightly, or moderately biodegraded oil samples (Fig. 4e–g). It is held that 25-norhopanes might originate from direct microbial degradation of hopanes (Peters et al., 1996; Chen et al., 2003; Huang, 2017a; Cheng et al., 2018). The 25-norhopanes with carbon number of 28–31 may be from biodegraded hopanes with carbon number of 29–32, which was consistent with that decreasing ratios of Gam/C_{30}H (gammacerane/C_{30} 17α(H)-hopane) and Gam/C_{31}H(S+R) (gammacerane/17α(H), 21β(H)–30–homohopane (22S + 22R)) with depth, as shown in Fig. 5d, e. Considering the occurrence frequency of 25-norhopanes, the highest biodegradation degree of this study area could be deemed as heavy, but not up to very severe.

Abundant tricyclic terpanes with carbon number from 19 to 29 were readily detected on the m/z 191 mass chromatograms (Fig. 4 i to l). Tricyclic terpanes appeared to present similar distribution characteristics even though they underwent different degrees of biodegradation. Tricyclic terpanes with carbon numbers from 19 to 24 were more abundant than those with carbon munbers from 26 to 29. Tricyclic terpanes were substantially more resistant to biodegradation than normal, branched hydrocarbons, and acyclic isoprenoids (Peters et al., 2005; Wang et al., 2013; Chang et al., 2018). Because of this, tricyclic terpanes with carbon numbers ranging from 23 to 29 still had high abundances, even though crude oil had been heavily biodegraded.

5α(H), 14α(H), 17α(H)–C_{27} sterane(20S) (C_{27}S, abbreviated similarly hereinafter), 5α(H), 14α(H), 17α(H)–C_{28} sterane(20S) (C_{28}S), and 5α(H), 14α(H), 17α(H)–C_{29} sterane(20S) (C_{29}S) presented similar characteristics on the m/z 217 mass chromatograms, noted that $C_{27}S<C_{28}S<C_{29}S$. However, the increasing trend from C_{27}S to C_{28}S to C_{29}S of oil in different biodegradation degrees still had differences. When slight biodegradation occurred, as shown in Fig. 4m, the increasing trend from C_{27}S to C_{28}S to C_{29}S presented itself like a mirrored "L". As biodegradation became stronger, the rising slope from C_{27}S to C_{28}S became steeper (Fig. 4 n, o). The increasing trend from C_{27}S to C_{28}S to C_{29}S turned into a similar shape of ascending straight line in the heavily biodegraded oils (Fig. 4p). The different trends of relative abundance between C_{27}S, C_{28}S, and C_{29}S in crude oils may be a response to biodegradation in different degrees. The susceptibility of steranes to biodegradation typically decreased with increasing carbon number for each isomeric configuration (Seifert et al., 1984; Peters et al., 2005). Therefore, C_{27}S usually degraded faster than C_{28}S and C_{29}S, and the relative abundance of C_{27}S was lower in heavily biodegraded oils than that in very slightly biodegraded oils. In summary, the effect of biodegradation on oils could be effectively unveiled through the GC and GC-MS. The real shapes of GC and GC-MS of crude oils without biodegradation may be more similar to Fig. 4a, e, i, m.

4.1.3. Biomarker parameters

As showed above, microbial selective degradation could, to a large extent, cloud the tracing and evaluation of biomarkers. Previous investigations claimed that Pr/nC_{17}, Ph/nC_{18} (Bao et al., 2002a,b; Dou et al., 2005), Gam/C_{30}H, Gam/C_{31}H (Bao et al., 2002a,b) increase and Pr/Ph (Dou et al., 2005; Bao et al., 2007) decreases with the increasing of biodegradation. The influence of biodegradation on these susceptible biomarker parameters should

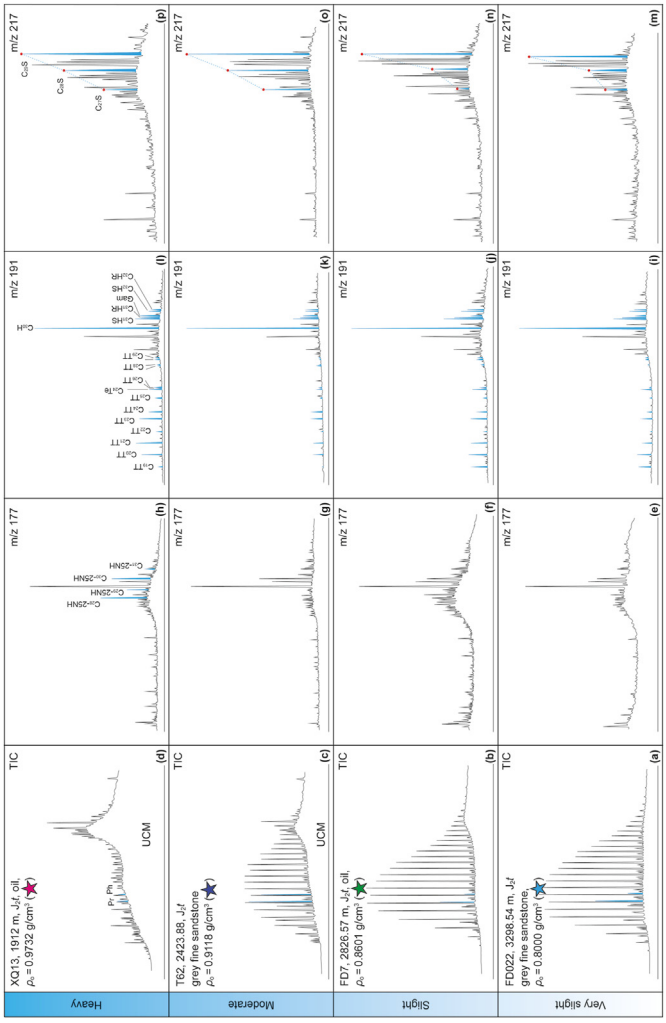

Fig. 4. TIC gas chromatogram, m/z 177, m/z 191, and m/z 217 mass chromatogram of oils in the Toutunhe Formation. Pr = pristine; Ph = phytane; C_i 25-NH = C_i 17α-25-norhopane, i = 28 to 31; C_i TT = C_i tricyclic terpane, i = 19 to 26, 28, 29; C_{24}Te = C_{24}tetracyclic terpane; C_{30}H = C_{30} 17α(H)-hopane; C_{31}HS = 17α(H), 21β(H) −30−homohopane (22S); C_{31}HR = 17α(H), 21β(H)-30−homohopane (22R); C_{32}HS = 17α(H), 21β(H)-30, 31−homohopane (22S); C_{32}HR = 17α(H), 21β(H)-30, 31−homohopane (22R); Gam = Gammacerane; C_i S = 5α(H), 14α(H), 17α(H)−C_i sterane (20S), i = 27 to 29. The pentagrams in color red, dark blue, green, and sky blue represented respectively the samples at the depth 1912 m of Well XQ13, 2423.88 m of Well T62, 2826.57 m of Well FD7, and 3298.54 m of Well FD022.

be taken into consideration in oil-source correlation (Bao et al., 2002a,b). Hence, in order to enhance the reliability of oil-source correlation of biodegraded oil, it is crucial to validate the biomarker parameters that remain inert to biodegradation. Reservoir temperature is a major factor that controls biodegradation. Biodegradation of petroleum is usually strongest at or near surface and tend to weaken with depth (Peters et al., 2005; Bennett et al., 2013). Furthermore, the relationship between biomarker parameters and depths was analyzed as shown in Figs. 5 and 6. The results demonstrated that several biomarker parameters commonly used for oil-source correlation showed good correlation with oil density and depth. Firstly, in either Santai or Fudong Oilfield, oil densities decrease with depth. The densities of oil samples from below 2,500 m in Santai Oilfield below 2,500 m ranged from 0.900 to 1.000 g/cm^3, while most of oil samples over 2,500m in Fudong Oilfield had smaller densities ranging from 0.800 to 0.900 g/cm^3 (Fig. 5a). Secondly, the Pr/nC$_{17}$, Gam/C$_{30}$H, and Gam/C$_{31}$H(S+R) ratios correlated negatively with depth and positively with oil density (Fig. 5b, d, e). The Pr/Ph ratios showed strong positive correlation with both depth and density (Fig. 5c). Changes of these biomarker parameters were mostly likely caused by the selective biodegradation of organic molecules. Normal alkanes are more susceptible to biodegradation than acyclic isoprenoids such as pristane and phytane (Schaefer and Leythaeuser, 1980; Peters et al., 2005). According to this, nC$_{17}$ degrades faster than pristane, and the Pr/nC$_{17}$ ratios increase as biodegradation exacerbates. Similarly, the gammacerane has higher resistance to biodegradation than C$_{30}$ 17α(H)-hopane, 17α(H), 21β(H)−30−homohopane (22S), and 17α(H), 21β(H)−30−homohopane (22R) (Peters et al., 2005; Huang, 2017). Besides, selective biodegradation of the pristane typically occurs at a higher rate because it has a lower carbon number than the phytane. Although Pr/nC$_{17}$, Pr/Ph, Gam/C$_{30}$H, and Gam/C$_{31}$H(S+R) ratio are commonly used as reliable biomarker parameters for oil-source correlation, unfortunately, normal alkanes, pristane, phytane, C$_{30}$-17α(H)-hopane, 17α(H), and 21β(H)−30−homohopane are evidently prone to be selectively degraded, especially when the biodegradation degree is anywhere above moderate. In this paper, it was concluded that these biomarker parameters may be less powerful to determine the source of biodegraded oil. Thus, in this case, it was essential to single out more reliable biomarker parameters to trace the source of biodegraded crude oil.

By comparison, the C$_{19}$−C$_{45}$ tricyclic terpanes and tetracyclic terpanes are highly resistant to biodegradation, which could survive even when hopanes are gone (Palacas et al., 1986; Peters et al.,

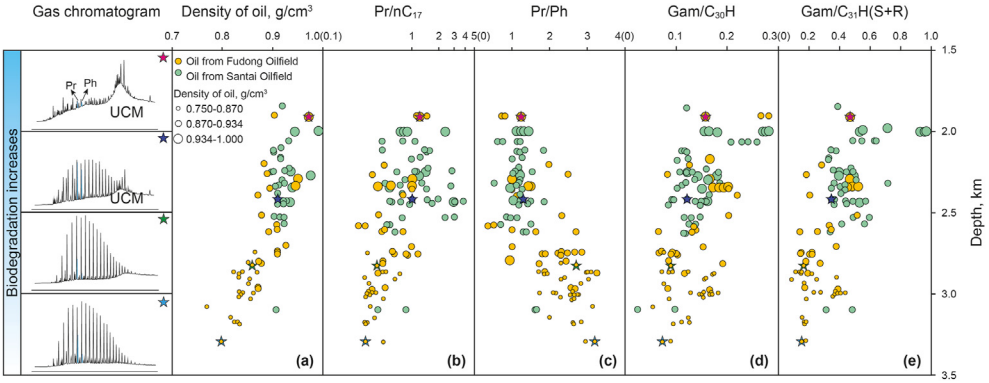

Fig. 5. Density and biomarker parameters versus depth showing significant effect of biodegradation on density, Pr/nC$_{17}$, Pr/Ph, Gam/C$_{30}$H, and Gam/C$_{31}$H(S+R). The pentagrams in color red, dark blue, green, and sky blue had the same indications in Fig. 4.

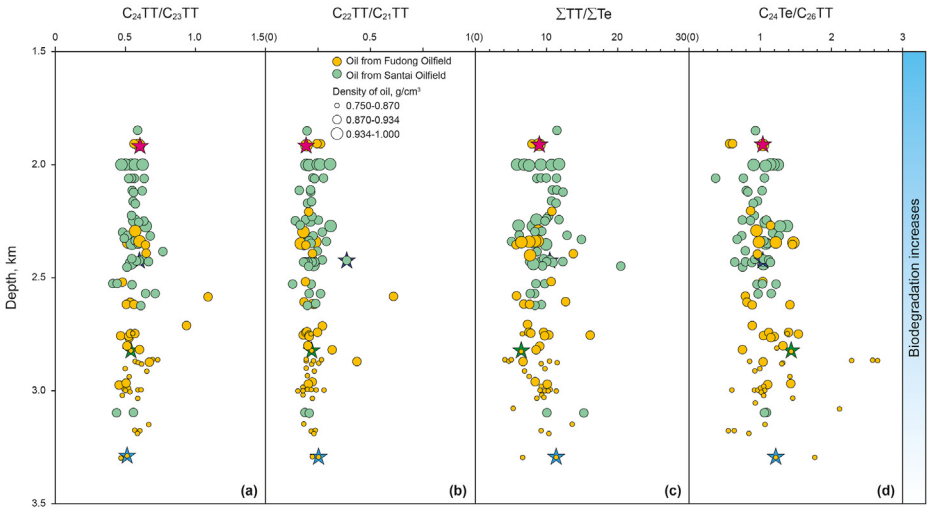

Fig. 6. Biomarker parameters versus depth showing significant effect of biodegradation on $C_{24}TT/C_{23}TT$, $C_{22}TT/C_{21}TT$, $\sum TT/\sum Te$, and $C_{24}Te/C_{26}TT$. The pentagrams in color red, dark blue, green, and sky blue had the same indications in Fig. 4.

2005). Several parameters with respect to tricyclic and tetracyclic terpanes such as C_{24} tricyclic terpane/C_{23} tricyclic terpane ($C_{24}TT/C_{23}TT$), C_{22} tricyclic terpane/C_{21} tricyclic terpane ($C_{22}TT/C_{21}TT$), $\sum$ tricyclic terpanes/$\sum$ tetracyclic terpanes ($\sum TT/\sum Te$), and C_{26} tricyclic terpane/C_{24} tricyclic terpane ($C_{24}Te/C_{26}TT$) were found to be more inert to biodegradation. It could be seen from Fig. 6a, b, c & d that these parameters changed within certain ranges, but remained no obvious correlation with biodegradation degree. The $C_{24}TT/C_{23}TT$ ratios mainly ranged from 0.5 to 0.7 with an average value of 0.58 (Fig. 6a). Similarly, most of the $C_{22}TT/C_{21}TT$ ratios were concentrated between 0.1 and 0.3 with an average value of 0.23 (Fig. 6b). In spite of different degree of biodegradation, the $\sum TT/\sum Te$ ratios did not change much with depth. Although the oils from Santai Oilfield suffered more from biodegradation than those from Fudong Oilfield, their $\sum TT/\sum Te$ ratios were still similar, most of them ranging between 6 and 12 with an average value of 9.30 (Fig. 6c). $C_{24}Te/C_{26}TT$ ratios of Fudong oils presented relatively more scattered than those of Santai oils. However, these ratios did not show significant correlation with biodegradation degree, but most of them changed in the range of 0.7–1.4 (Fig. 6d). For validation purpose, four typical $C_{24}Te/C_{26}TT$ ratios representing different degree of biodegradation were selected for comparison. At the depths of 1912 m, 2423.25 m, 2813 m and 3298.54 m, the ratio was 1.05, 0.93, 1.24 and 1.23 respectively, fitting in a very tight range (Fig. 6d). All in all, these tricyclic terpanes and tetracyclic terpanes ratios maintained high stability regardless of biodegradation degree. In other words, these parameters that were inert to biodegradation, could be used as effective biomarker parameters for oil-source correlation.

In summary, the oil in this study area was typically biodegraded to different extent from very slight to heavy. The degree of biodegradation decreased with buried depth of oil samples. The highest biodegradation degree could be deemed as heavy, but not up to a very severe degree. The most of oil from Santai Oilfield underwent moderate to heavy biodegradation, while that from Fudong Oilfield underwent moderate to slight biodegradation, in other words, oil from Santai Oilfield suffered more from biodegradation than that from Fudong Oilfield.

4.2. Potential source rock

4.2.1. Hydrocarbon generation potential

There were four hydrocarbon generative source rocks of Carboniferous, Permian, Triassic, and Jurassic age in the eastern Junggar Basin (Fig. 1b). The total organic carbon (TOC) content of P_2l ranged from 0.46% to 6.72% with a mean value of 1.84%. The S_1+S_2 value of the source rock samples was in the range of 0.36–26.28 mg HC/g rock with an average value of 5.02 mg HC/g rock. This indicated that the source rocks had high organic matter abundance. Most of the $T_{2\text{-}3}xq$ source rock samples had TOC contents greater than 0.6%, and S_1+S_2 values over 1.0 mg HC/g rock, reflecting slightly lower organic matter abundance than P_2l source rock. The Jurassic source rocks, by contrast, had the lowest organic matter abundance with 0.3%–2.09% (0.87% on average) TOC, and 0.06–3.55 mg HC/g rock (1.22 mg HC/g rock on average) S_1+S_2 (Fig. 7a). Cross-plots of T_{max} versus HI (S_2/TOC) showed that P_2l and $T_{2\text{-}3}xq$ source rocks were dominated by type II kerogen, the difference being $T_{2\text{-}3}xq$ source rocks having a higher content of type II_2 organic matter. The organic matter type of Jurassic source rocks was mainly type II_2 and III, reflecting the gas-prone potential (Fig. 7b). Owing to the high abundance and type II organic matter, the P_2l source rocks were believed to generate a considerable amount of oil, and were the best source rocks in this area, followed by $T_{2\text{-}3}xq$ source rock. Due to lower organic matter abundance and gas-prone organic matter type, Jurassic source rocks were considered to be with limited potential to generate oil. The Carboniferous source rocks mainly composed of mudstone and tuffaceous mudstone, with main organic matter type III, having great gas generative potential, as investigated by explorers that the gas of Kelameili Gasfield located in Eastern Junggar Basin originated from Carboniferous source rocks (Yuan et al., 2015; Xiang et al., 2016). Therefore, the Jurassic and Carboniferous source rocks may not be the primary oil source for Fudong and Santai oilfields. Besides, Fudong and Santai Oilfield were located near or within the pinchout line of P_2l source rock (Fig. 1a), consequently, the in-situ source rocks in oilfield areas were thin or absent. So as a conclusion, the deep depression zone, rather than the autochthonous area where oilfields were located, was supposed to be the primary area for P_2l source rock to generate substantial amount of oil.

Further, in order to define the time when the source rocks reached oil window as well as the peak of oil generation,

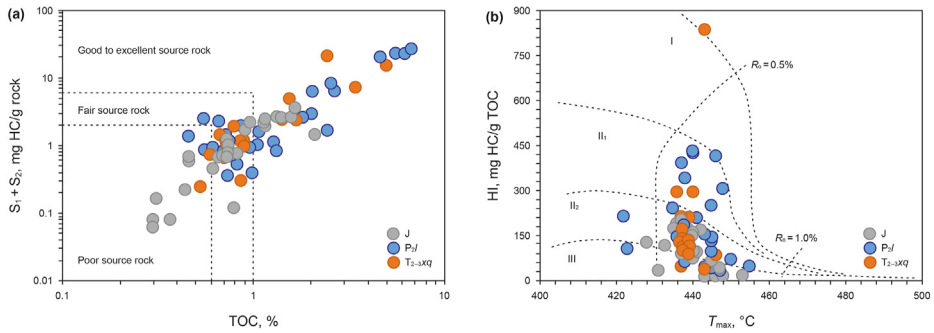

Fig. 7. Characteristics of P_2l, $T_{2\text{-}3}xq$, and Jurassic source rocks. (a) cross-plot of S_1+S_2 versus TOC content showing hydrocarbon generation potential of source rocks; (b) cross-plot of HI (hydrogen index) versus T_{max} showing different types of kerogen and their maturities.

reconstructing hydrocarbon generation histories of source rocks was carried out based on BasinMode Software. The input data in the simulation involved present-day strata thickness, lithology, depth, and temperature. Geochemical input parameters for modelling including TOC, R_o and Rock-Eval pyrolysis data. Maturity was calculated using the Easy% R_o model of Sweeney and Burnham (1990). Organofacies for P_2l, and $T_{2\text{-}3}xq$ source rocks were assigned as Type II (BMOD-1D LLNL), while Type III (BMOD-1D LLNL) was assigned to the Jurassic source rock. The modelling results showed that the P_2l source rocks reached oil window at 190 Ma (Early Jurassic) and oil generation peak at about 164 Ma (Middle-Late Jurassic), while the Triassic source rocks reached the oil window and oil generation peak at about 104 Ma (Middle Cretaceous) and 91 Ma (Middle Cretaceous) respectively (Fig. 8, Fig. 9). By comparison, the Jurassic source rocks matured late, although their burial depths of Jurassic source rocks exceeded 4,800 m (e.g. Well D6), and their present-day R_o values were as low as 0.64%–1.08% with an average value of 0.77%. The burial and thermal history of Well D6 showed that the earliest time when the Jurassic source rocks reached oil window was the Early Paleogene (Fig. 10), which was apparently later than P_2l and $T_{2\text{-}3}xq$ source rocks.

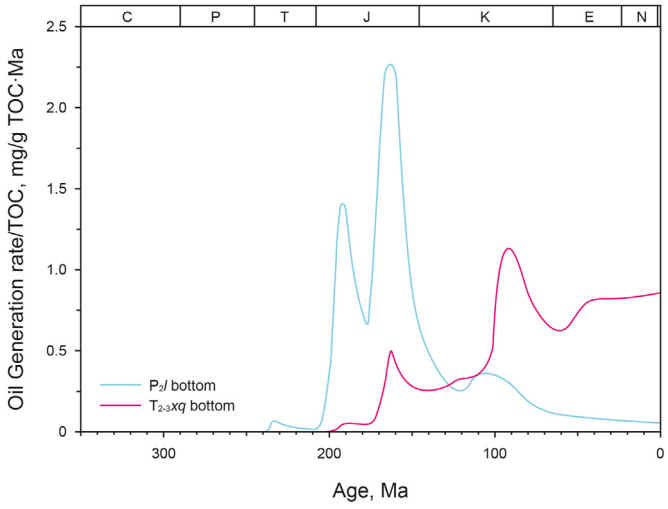

Fig. 9. Oil generation history of P_2l and $T_{2\text{-}3}xq$ source rocks.

4.2.2. Carbon isotopes and biomarkers

Carbon isotopes of oil generated by organic matter biologically sourced from terrestrial higher plants are typically heavier than that from lower organisms (Aichner et al., 2010). The carbon isotopes of P_2l source rocks were the lowest ranging from −33.32‰ to −28.76‰ with the mean value of −30.78‰, followed by those of $T_{2\text{-}3}xq$ source rocks ranging from −31.79‰ to −27.48‰ with the mean value of −29.59‰ (Fig. 11). Whereas, the Jurassic source rocks had relatively higher carbon isotopes ranging from −29.60‰

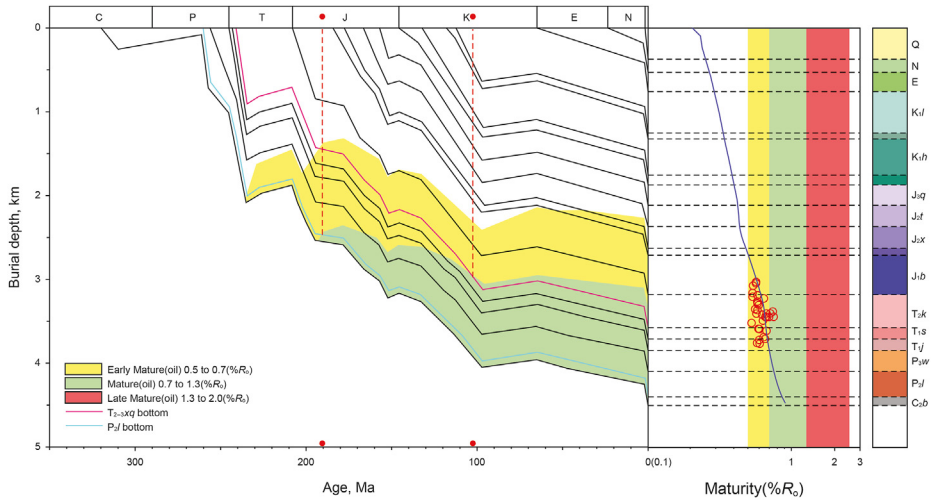

Fig. 8. Burial and thermal history of Well Fu10 showing the times when P_2l and $T_{2\text{-}3}xq$ source rocks reached the oil window.

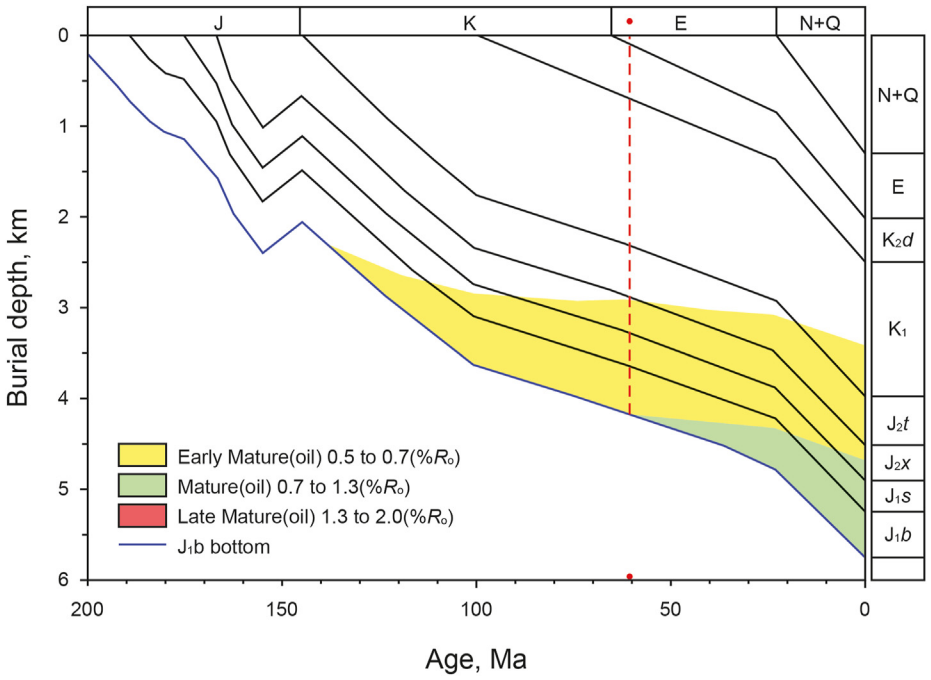

Fig. 10. Burial and thermal history of Well D6 showing the earliest time when Jurassic source rocks reached the oil window.

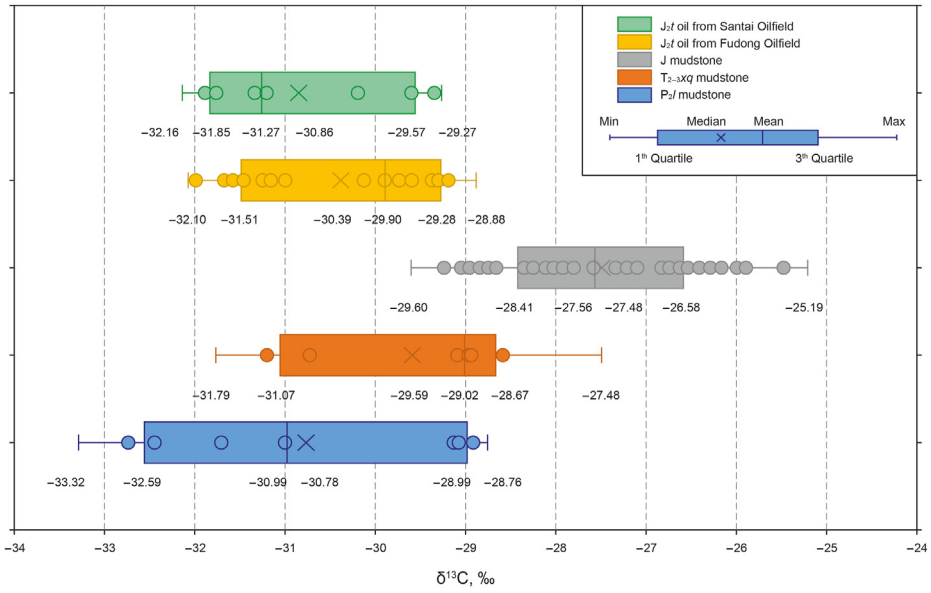

Fig. 11. Carbon isotopes of chloroform extracts from P_2l, $T_{2\text{-}3}xq$, Jurassic source rocks and oil-bearing sandstones showing differences between source rocks and correlation between source rocks and oil.

to −25.19‰ with the mean value of −27.49‰, which indicated that organic matter in the Jurassic source rocks predominantly sourced from terrestrial higher plants. This conclusion could be supported by the discovery of coal seams in the Jurassic strata (Fig. 1c).

As mentioned above, due to greater resistance to biodegradation, tricyclic terpanes with carbon number of 21–24 were selected for oil-source correlation. A cross plot of $C_{24}TT/C_{23}TT$ versus $C_{22}TT/C_{21}TT$ was drawn to differentiate between P_2l and $T_{2\text{-}3}xq$ source rocks (Fig. 12). On the plot, it was clear that the $T_{2\text{-}3}xq$ source rocks had higher values of $C_{24}TT/C_{23}TT$ and $C_{22}TT/C_{21}TT$ than P_2l source rocks. $C_{24}TT/C_{23}TT$, $C_{22}TT/C_{21}TT$ ratios of $T_{2\text{-}3}xq$ source rocks ranged from 0.54 to 0.93 with an average of 0.67, 0.12–0.36 with an average of 0.23, while $C_{24}TT/C_{23}TT$, $C_{22}TT/C_{21}TT$ ratios of P_2l source rocks were smaller ranging from 0.26 to 0.71 with an average of 0.42, and 0.05–0.29 with an average of 0.15 respectively.

Tricyclic terpanes are generally believed to derive mainly from algae and bacteria (Fu et al., 2009; Duan et al., 2009), while terrigenous organic matter has relatively high C_{24} tetracyclic terpane abundance (Zhang and Huang, 2005; Duan et al., 2009). The $\sum TT/\sum Te$ and $C_{24}Te/C_{26}TT$ ratios of $T_{2\text{-}3}xq$ and P_2l source rocks presented great differences, as shown in Fig. 13. Most of $C_{24}Te/C_{26}TT$ ratios of $T_{2\text{-}3}xq$ source rocks ranged from 1 to 10, while those

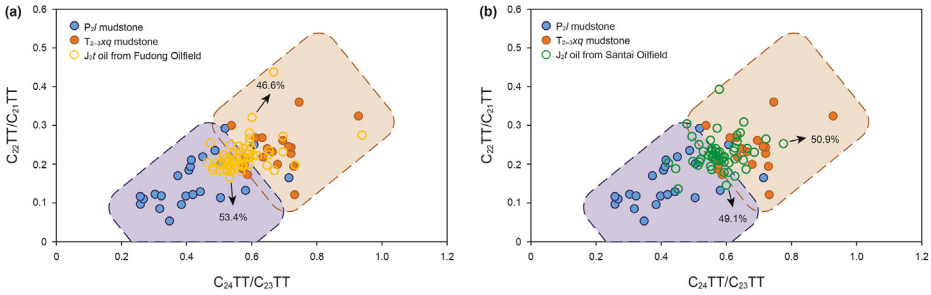

Fig. 12. $C_{24}TT/C_{23}TT$ versus $C_{22}TT/C_{21}TT$ showing difference between source rocks and correlation between source rocks and Fudong oil (a) or Santai oil (b).

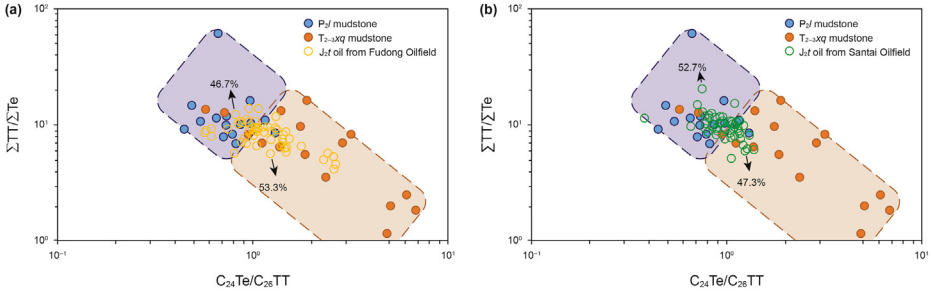

Fig. 13. $C_{24}Te/C_{26}TT$ versus $\sum TT/\sum Te$ showing difference between source rocks and correlation between source rocks and Fudong oil (a) or Santai oil (b).

of P_2l source rocks were mostly below 1. Similarly, the $\sum TT/\sum Te$ ratios of $T_{2\text{-}3}xq$ source rocks ranged from 1.23 to 17.07 with an average of 8.07, while P_2l source rocks ratios were substantially higher, with a minimum value of 7.02, a maximum value of 62.79 and an average value of 14.33. P_2l source rocks had relatively larger $\sum TT/\sum Te$ ratios and smaller $C_{24}Te/C_{26}TT$ ratios than those of $T_{2\text{-}3}xq$ source rocks (Fig. 13). Therefore, it could be concluded that the organic matter of P_2l source rocks may have more algae and bacteria input, and this was consistent with its lighter carbon isotope (Fig. 11).

4.3. Oil-source correlation

In this paper, carbon isotope, reliable biomarkers, and oil accumulation history were combined to correlate oil and source rocks. Carbon isotope analysis of chloroform extracts from P_2l, $T_{2\text{-}3}xq$, Jurassic source rocks and oil-bearing sandstones was carried out to show differences between source rocks and correlation between source rocks and oils. The carbon isotope values of oil-bearing sandstones from Santai Oilfield and Fudong Oilfield mainly ranged from −31.85‰ to −29.57‰, −31.51‰ to −29.28‰ and with mean values of −30.86‰, −30.39‰ respectively. The majority of carbon isotope values of Jurassic source rocks was in the range of −28.41‰ – −26.58‰ with an average of −27.48‰. Clearly, the carbon isotope values of oil-bearing sandstones were 1–3‰ heavier than the majority of these of Jurassic mudstones, which revealed poor correlation between J_2t oil and Jurassic source rocks. Additionally, a much later oil window of Jurassic source rocks could exclude the possibility that the Jurassic source rocks could be oil source for the J_2t reservoirs. The earliest time for Jurassic source rocks to reach the oil window was the Early Paleogene (Fig. 10), whereas the charging times of J_2t reservoirs recorded by fluid inclusions were before the Late Cretaceous. Therefore, oil in J_2t was more likely sourced from P_2l or/and $T_{2\text{-}3}xq$ mudstone rather than Jurassic mudstone.

Further, for the sake of determining the precise source of biodegraded oil in J_2t, preferable biomarker parameters were optimized to correlate the P_2l, $T_{2\text{-}3}xq$ mudstone and oils. As previously discussed, the cross plots of $C_{24}TT/C_{23}TT$ versus $C_{22}TT/C_{21}TT$ and $C_{24}Te/C_{26}TT$ versus $\sum TT/\sum Te$ were perfectly effective to differentiate the characteristics of P_2l and $T_{2\text{-}3}xq$ source rocks. As can be seen from Figs. 12 and 13, these biomarker ratios of oil from Santai or Fudong Oilfield changed in a limited scale, but distributed in shaded areas of two source rocks. As can be seen from Figs. 12a and 46.6% of oils from Fudong oilfield distributed in the $T_{2\text{-}3}xq$ source rock area, while 53.4% of them distributed in the P_2l source rock area. Similarly, oils from Santai oilfield approximately equally distributed in the $T_{2\text{-}3}xq$ and P_2l source rock areas, which accounted for 50.9% and 49.1% respectively (Fig. 12b). From Fig. 13a, oils from Fudong oilfield distributed in the $T_{2\text{-}3}xq$ source rock area accounted for 53.3%, and that distributed in the P_2l source rock area accounted for 46.7%. Oils from Santai oilfield distributed in the $T_{2\text{-}3}xq$ source rock area accounted for 47.3%, and the proportion of that distributed in the P_2l source rock area was 52.7% (Fig. 13b). These biomarker ratios of oils from Santai or Fudong Oilfield changed in a limited scale, but approximately equally distributed in shaded areas of two source rocks. It indicated that oils in these two oilfields originated from both two source rocks rather than one of them.

4.4. Oil accumulation history

A more accurate approach of tracing oil source shall not only analyze the affinity of biomarkers, but also involve the geological reality of reasonable history match with oil generation and oil charging. Therefore, core sample observation, microscopic fluorescent analysis and fluid inclusion analysis were all integrated to perform a comprehensive analysis of the charging history and accumulation process of oil. A substantial solid bitumen was found in the dissolved pores or cracks of oil-bearing sandstone core samples (see Fig. 14), which indicated that solid bitumen was a response to biodegradation as mentioned above.

Hydrocarbons emit fluorescence under ultraviolet light, and the

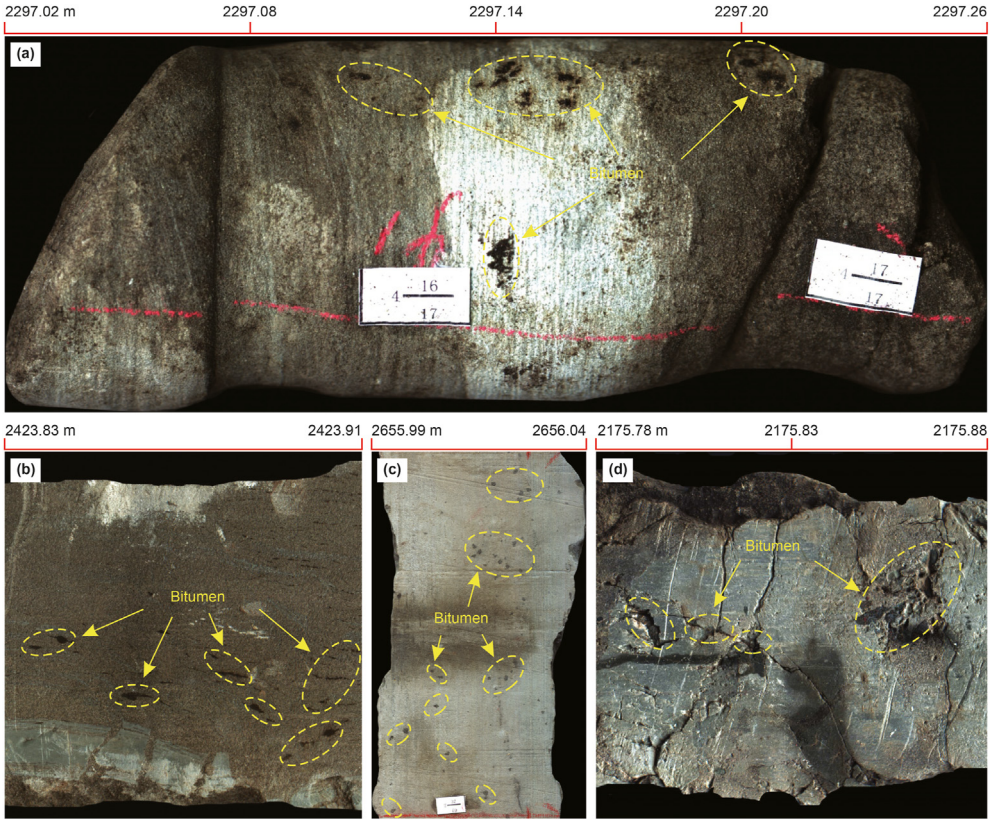

Fig. 14. Oil-bearing sandstone core samples with black solid bitumen showing biodegradation. Sample A (a): Bei 95, 2297.02–2297.26m, J_2t, oil-bearing sandstone; Sample B (b): Tai 62, 2423.83–2423.91m, J_2t, oil-bearing sandstone; Sample C (c): FD081, 2655.99–2656.04m, J_2t, oil-bearing sandstone; Sample D (d): Tai102, 2175.78–2175.88m, J_2t, oil-bearing sandstone.

fluorescent colors vary with different bulk composition and maturity. Therefore, fluorescence is commonly used to investigate hydrocarbon migration and charging stage (Lin et al., 2017; Si et al., 2013). Multi-stage oil charging could lead to the coexistence of hydrocarbons with different fluorescent colors (Eadington et al., 1991). The microscopic fluorescent photographs a-e in Fig. 15 were from J_2t reservoirs of the Fudong Oilfield, the photographs h-l were from the reservoir of the Santai oilfield, and the photographs f-g were from wells between the two oilfields. Among all these photographs, two fluorescence colors coexisted regardless of well location. One fluorescent color was light brown to dark brown, while another one was blue to blueish white. These two distinct fluorescent colors reflected that oil in the Toutunhe Formation was mixture originated from at least two charging stages. Taking aforementioned oil biodegradation into account, we believed that the light brown to dark brown fluorescence corresponded to the residual bitumen formed from biodegradation in the first charging stage, while blue to blueish white fluorescence corresponded to normal non-biodegraded oil in the later charging stage. Two distinct colors of fluorescence coexisted in J_2t reservoirs of almost all wells, nonetheless, there were some identifiable differences in the fluorescence colors of reservoirs in different blocks. The fluorescent color of bitumen in the core thin sections from Fudong Oilfield was lighter, showing light brown or tawny (Fig. 15a–e), while that from Santai Oilfield (Fig. 15h–l) and other in-between wells (Fig. 15f to g) looked darker with a dark brown or chocolate color. Moreover, more bitumen was detected in Santai wells and in-between wells (B95 and B24) than Fudong wells. Particularly, when observing a thin section from Well T59 under the microscope, bitumen was found to have filled literally all the intergranular pores (Fig. 15l), leaving every mineral particle easily visible in the horizon, while blue to blue-white fluorescence presenting normal oil was only observed in the intragranular pores. The differences in the bitumen color and content between the two oilfields may be caused by the more serious biodegradation of oil charged in the first stage from Santai Oilfield. This result was consistent with the fact that Santai oilfield has higher oil density and viscosity, lower saturated hydrocarbon content, lower Pr/Ph, higher Gam/C_{30}H and Gam/C_{31}H(S+R) ratios.

In the process of reservoir diagenesis, fluid inclusions often occurred during the formation of cements and secondary minerals. The homogenization temperature (Th) of brine inclusions that were formed concurrently with hydrocarbon inclusions represented the temperature at which hydrocarbons charged into the reservoir. Based on this temperature, the paleogeothermal model of the basin and the burial history of the reservoir, the depth and corresponding geological age could be determined for the formation of fluid inclusion (Volk et al., 2005; Cao et al., 2006; Liu et al., 2016). The homogenization temperatures of fluid inclusions in Well B81 were tested and 37 temperature points were obtained. The temperatures ranged from 28.9 °C to 86.6 °C with two peaks near 40–50 °C and 80–90 °C (see Fig. 16), suggesting that two possible oil charging stages ever occurred within these two temperature ranges. Further, the burial and geothermal history of Well B81 was simulated using the Software Basinmod, and the results were shown in Fig. 16. According to homogenization temperatures, burial and geothermal history, two oil charging stages were recognized: the first stage was from the End Jurassic to the Early Cretaceous (about 146 Ma to 133 Ma), and the second stage dated back to the Middle Cretaceous (about 103 Ma to 90 Ma). The geological time of the first oil

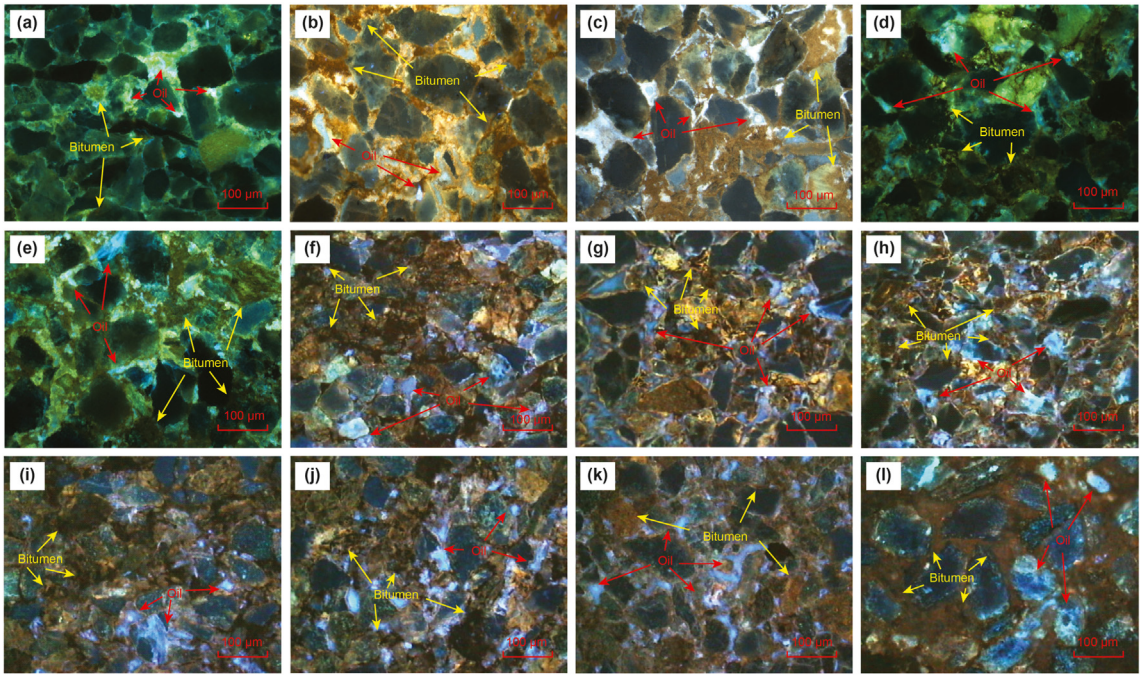

Fig. 15. The microscopic fluorescent photographs of the Toutunhe Formation reservoirs showing multiple oil charging stages. (a). FD071, 3144.94m, J_2t, gray fine sandstone; (b). FD11, 2943.76m, J_2t, gray fine sandstone; (c) FD161, 2053.48m, J_2t, gray medium to fine sandstone; (d). FD081, 2656.43m, J_2t, gray fine sandstone; (e). FD081, 2707.08m, J_2t, gray fine sandstone; (f).B95, 2297.40m, J_2t, gray fine sandstone; (g)., B24, 2013.97m, J_2t, gray fine sandstone; (h). XD1, 1996.91m, J_2t, gray fine sandstone; (i). T17, 1964.70m, J_2t, gray fine sandstone; (j). T17, 1964.30m, J_2t, gray fine sandstone; (k). T38, 2428.03m, J_2t, gray medium to fine sandstone; (l). T59, 3010.01m, J_2t, gray medium sandstone.

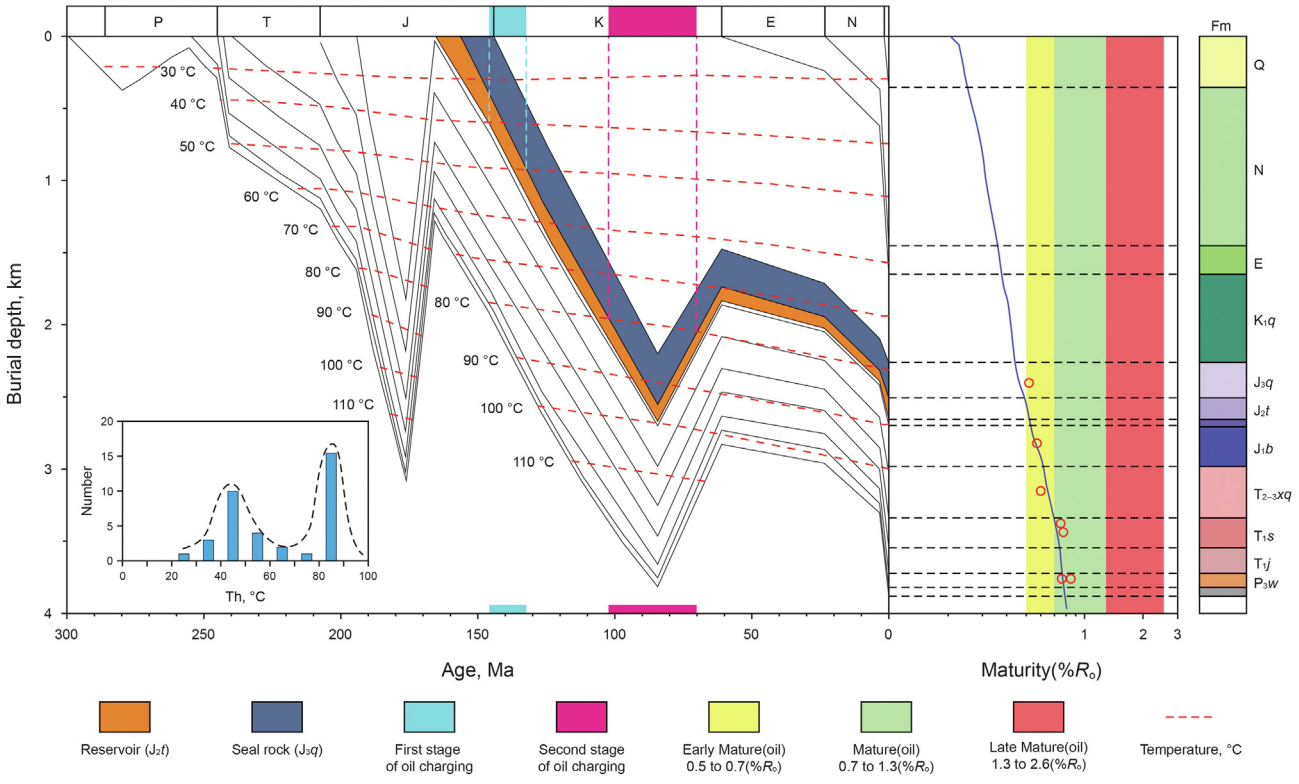

Fig. 16. The homogenization temperatures, burial and geothermal history of Well B81 showing two stages of oil charging for the Toutunhe Formation.

charging stage coincided with the oil generation peak of P_2l source rock, indicating that the oil in J_2t reservoir charged in the first charging stage originated from P_2l source rock. Likely, the geological time of the second oil charging stage matched the oil generation peak of $T_{2\text{-}3}xq$ source rock, indicating that the oil in J_2t reservoir charged in the second charging stage originated from $T_{2\text{-}}$

$_3xq$ source rock.

Based an integrated study on oil biodegradation, source, and oil charging history, the whole process of oil accumulation has been thoroughly investigated and understood. The oil accumulation model could be outlined as follows. The P_2l source rock reached oil window at 190 Ma (Early Jurassic) and oil generation peak at about 164 Ma (Middle-Late Jurassic). Then generated oil migrated from the deep depression area to the slope area along the east-west oriented faults and unconformities, and was finally trapped in the J_2t reservoirs in the first oil charging stage roughly between 146 Ma and 133 Ma. However, as seen from Fig. 16, during the 20 Ma before oil charging, the strata had risen sharply. So when the oil was charged into the reservoirs, the buried depth of J_2t was only about 600 m–900 m, and the reservoir temperature was 40 °C–50 °C, which was considered ideal for microbial degradation of oil (Peters et al., 2005; Bennett et al., 2013). At the meantime, as the seal rocks of J_2t reservoir, the overlying Qigu Formation (J_3q) just began to deposit. Consequently, the thickness of the overlying rocks was too small to seal the underlying oil accumulation effectively. As a result of this, the oil originated from P_2l source rock was biodegraded into bitumen, as shown in Figs. 14 and 15. Subsequently the strata subsided, hence a much deeper depth of J_2t reservoir. The $T_{2\text{-}3}xq$ source rock reached oil window at about 104 Ma, and oil generation peak at about 91 Ma. In this time window, the reservoirs were recharged by oil generated from Triassic source rocks, leaving the already biodegraded oil mixed with oil from the Triassic source rock.

5. Conclusions

The oil of Toutunhe Formation of Jurassic in the eastern Junggar Basin was biodegraded to different extent, which resulted in the increase of oil density and the decrease of saturated hydrocarbon content. When very slightly or slightly biodegraded, the oil was characterized as slightly broken down *n*-alkanes, as well as the absence of prominent chromatographic baseline hump and 25-norhopanes. Moderate to heavy biodegradation typically occurred with partially broken down *n*-alkanes, obvious baseline hump, and possible existence of 25-norhopanes. Furthermore, heavy biodegradation undermined the reliability of biomarker parameters commonly used for oil-source correlation in that the ratios of Pr/nC_{17}, Gam/C_{30}H, Gam/C_{31}H(S+R) tended to increase and Pr/Ph tended to decrease with biodegradation degree.

Nonetheless, ratios of C_{24}TT/C_{23}TT, C_{22}TT/C_{21}TT, $\sum$TT/$\sum$Te, and C_{24}Te/C_{26}TT remained relatively stable and correlated poorly with biodegradation degree, so these biomarker parameters were demed more powerful for oil-source correlation. The combined study of selected reliable biomarker parameters and carbon isotopes revealed that biodegraded oil in J_2t probably originated from the P_2l and $T_{2\text{-}3}xq$ source rocks rather than the Jurassic source rocks because the latter featured higher carbon isotope values and ill-timed hydrocarbon generation history.

The P_2l source rocks reached oil window at 190 Ma (Early Jurassic), and oil generation peak at 164 Ma (Middle-Late Jurassic). Subsequently, generated oil migrated eastward from the depression area to slope area along the west-east oriented faults and unconformities. Between about 146 Ma to 133 Ma, J_2t reservoirs were charged for the first time. But due to poor preservation condition, the accumulated oil was biodegraded to different extent and solid bitumen was formed when heavy biodegradation occurred. Later, at 104 Ma (Middle Cretaceous), the $T_{2\text{-}3}xq$ source rocks began to generate substantial amounts of oil and reached oil generation peak at 91 Ma (Middle Cretaceous). In this period, the J_2t reservoirs were recharged, thereafter the charged oil was mixed with the previous biodegraded oil. Therefore, the oil in J_2t reservoirs now was a mixture originated from the P_2l and $T_{2\text{-}3}xq$ source rocks during two separate charging stages.

Acknowledgments

This work was supported by a grant from National Science Foundation for Young Scientists of China (Grant No. 41702143), Natural Science Foundation of Shandong Province of China (ZR2016DL06; ZR2017LD005), the Fundamental Research Funds for the Central Universities (17CX02006A), the Foundation of Shandong Provincial Key Laboratory of Depositional Mineralization & Sedimentary Mineral (DMSM2017063), the major science and technology project of Xinjiang Petroleum Administration Bureau of CNPC (2017E-0401). We would like to thank the Xinjiang Petroleum Administration Bureau of CNPC for providing the core samples.

References

Abbott, G.D., Lewis, C.A., Maxwell, J.R., 1985. Laboratory models for aromatization and isomerization of hydrocarbons in sedimentary basins. Nature 318 (6047), 651–653. https://doi.org/10.1038/318651a0.

Aichner, B., Herzschuh, U., Wilkes, H., 2010. Influence of aquatic macrophytes on the stable carbon isotopic signatures of sedimentary organic matter in lakes on the Tibetan Plateau. Org. Geochem. 41 (7), 706–718. https://doi.org/10.1016/j.orggeochem.2010.02.002.

Bao, J., Zhu, C.S., 2009. The effects of biodegradation on the compositions of aromatic hydrocarbons and maturity indicators in biodegraded oils from Liaohe Basin. Sci. China Earth Sci. 52 (1 Suppl. ment), 59–68. https://doi.org/10.1007/s11430-009-5017-5.

Bao, J.P., Zhu, C.S., Ma, A.L., et al., 2002a. Quantitative study of biomarker composition in biodegraded oils. J. Jianghan Petrol. Inst. 24 (2), 22–26. https://doi.org/10.3969/j.issn.1000-9752.2002.02.007 (in Chinese).

Bao, Z.D., Guan, S.Z., Li, R.F., et al., 2002b. Sequence stratigraphy of the jurassic in Junggar Basin. Petrol. Explor. Dev. 29 (1), 48–51. https://doi.org/10.3321/j.issn:1000-0747.2002.01.012 (in Chinese).

Bao, J.P., Zhu, J.Z., Zhu, C.S., et al., 2007. A biodegradation experiment of crude oils in laboratory. Petrol. Explor. Dev. 34 (1). https://doi.org/10.3321/j.issn:1000-0747.2007.01.009, 43–47+112 (in Chinese).

Bennett, B., Adams, J.J., Gray, N.D., et al., 2013. The controls on the composition of biodegraded oils in the deep subsurface – part 3. the impact of microorganism distribution on petroleum geochemical gradients in biodegraded petroleum reservoirs. Org. Geochem. 56, 94–105. https://doi.org/10.1016/j.orggeochem.2012.12.011.

Cao, J., Yao, S.P., Jin, Z.J., et al., 2006. Petroleum migration and mixing in the northwestern Junggar Basin (NW China): constraints from oil-bearing fluid inclusion analyses. Org. Geochem. 37 (7), 827–846. https://doi.org/10.1016/j.orggeochem.2012.12.011.

Chang, X.C., Zhao, H.G., He, W.X., et al., 2018. Improved understanding of the alteration of molecular compositions by severe to extreme biodegradation: a case study from the carboniferous oils in the eastern chepaizi uplift, Junggar Basin, northwest China. Energy Fuels 32 (7), 7557–7568. https://doi.org/10.1021/acs.energyfuels.8b01557.

Chen, J.Y., Bi, Y.P., Zhang, J.G., et al., 1996. Oil-source correlation in the fulin basin, shengli petroleum province, east China. Org. Geochem. 24 (8–9), 931–940. https://doi.org/10.1016/s0146-6380(96)00049-6.

Chen, J.Q., Jiang, Z.X., Pang, H., et al., 2014. Lateral migration of petroleum in the jurassic Toutunhe Formation in the Fudong slope, Junggar Basin, China. Resour. Geol. 64 (1), 35–46. https://doi.org/10.1111/rge.12025.

Chen, J.P., Liang, D.G., Wang, X.L., et al., 2003. Mixed oils derived from multiple source rocks in the Cainan oilfield, Junggar Basin, Northwest China. Part I: genetic potential of source rocks, features of biomarkers and oil sources of typical crude oils. Org. Geochem. 34 (7), 889–909. https://doi.org/10.1016/S0146-6380(03)00030-5.

Cheng, X., Hou, D.J., Xu, C.G., 2018. The effect of biodegradation on adamantanes in reservoired crude oils from the Bohai Bay Basin, China. Org. Geochem. 123, 38–43. https://doi.org/10.1016/j.orggeochem.2018.06.008.

Dawson, K.S., Schaperdoth, I., Freeman, K.H., et al., 2013. Anaerobic biodegradation of the isoprenoid biomarkers pristane and phytane. Org. Geochem. 65, 118–126. https://doi.org/10.1016/j.orggeochem.2013.10.010.

Ding, X.J., Gao, C.H., Zha, M., et al., 2017. Depositional environment and factors controlling β-carotane accumulation: a case study from the Jimsar Sag, Junggar Basin, northwestern China. Palaeogeogr. Palaeoclimatol. Palaeoecol. 485, 833–842. https://doi.org/10.1016/j.palaeo.2017.07.040.

Ding, X.J., Liu, G.D., Imin, A., et al., 2018. Relationship between source rock development and petroleum accumulation in the Erlian Basin, northern China. Geol. J. 54 (10), 1–15. https://doi.org/10.1002/gj.3265.

Dou, Q.L., Chen, J.F., Xue, Y.F., et al., 2005. A comparative study of the geochemical characters of crude oil after microbe degradation in laboratory. Acta Sedimentol. Sin. 23 (3), 542–547. https://doi.org/10.3969/j.issn.1000-

0550.2005.03.023 (in Chinese).
Duan, Y., Wang, J.G., Wu, B.X., et al., 2009. Geochemical characteristics and genesis of crude oils from Gasikule Oilfield in western Qaidam Basin, China. Geochem. J. 43 (5), 293–304. https://doi.org/10.2343/geochemj.0.0166.
Eadington, P.J., Hamilton, P.J., Bai, G.P., 1991. Fluid history analysis - a new concept for prospect evaluation. APEA J. 31 (1), 282–294. https://doi.org/10.1071/AJ90022.
Emery, D., Robinson, A., 1993. Inorganic Geochemistry: Applications to Petroleum Geology. Blackwell Scientific Publications, London, pp. 41–71, 1993.
Fu, X.G., Wang, J., Zeng, Y.H., et al., 2009. Geochemical and palynological investigation of the shengli river marine oil shale (China): implications for paleoenvironment and paleoclimate. Int. J. Coal Geol. 78, 217–224. https://doi.org/10.1016/j.coal.2009.02.001.
Hakimi, M.H., Abdullah, W.H., 2015a. Modelling petroleum generation of late cretaceous dabut Formation in the jiza-qamar basin, eastern Yemen. Mar. Petrol. Geol. 61, 1–13. https://doi.org/10.1016/j.marpetgeo.2014.11.004.
Hakimi, M.H., Abdullah, W.H., 2015b. Thermal maturity history and petroleum generation modelling for the Upper Jurassic Madbi source rocks in the Marib-Shabowah Basin, western Yemen. Mar. Petrol. Geol. 59, 202–216. https://doi.org/10.1016/j.marpetgeo.2014.08.002.
Hao, F., Zhou, X.H., Zhu, Y.M., et al., 2011. Lacustrine source rock deposition in response to co-evolution of environments and organisms controlled by tectonic subsidence and climate, Bohai bay Basin, China. Org. Geochem. 42, 323–339. https://doi.org/10.1016/j.orggeochem.2011.01.010.
He, D.F., 2007. Structure of unconformity and its control on hydrocarbon accumulation. Petrol. Explor. Dev. 34 (2), 142–149. https://doi.org/10.3321/j.issn:1000-0747.2007.02.003.
Head, I.M., Jones, D.M., Larter, S.R., 2003. Biological activity in the deep subsurface and the origin of heavy oil. Nature 426 (6964), 344–352. https://doi.org/10.1038/nature02134.
Huang, H.P., 2017. The effect of biodegradation on gammacerane in crude oils. Biodegradation 28 (4), 313–326. https://doi.org/10.1007/s10532-017-9798-5.
Huang, H.P., Larter, S., 2014. Secondary microbial gas formation associated with biodegraded oils from the Liaohe Basin, NE China. Org. Geochem. 68, 39–50. https://doi.org/10.1016/j.orggeochem.2014.01.005.
Huang, H.P., Li, J., 2017. Molecular composition assessment of biodegradation influence at extreme levels – a case study from oilsand bitumen in the Junggar Basin, NW China. Org. Geochem. 103, 31–42. https://doi.org/10.1016/j.orggeochem.2016.10.005.
Hubert, C.R.J., Oldenburg, T.B.P., Fustic, M., et al., 2012. Massive dominance of Epsilonproteobacteria in formation waters from a Canadian oil sands reservoir containing severely biodegraded oil. Environ. Microbiol. 14 (2), 387–404. https://doi.org/10.1111/j.1462-2920.2011.02521.x.
Larter, S., Huang, H.P., Adams, J., et al., 2006. The controls on the composition of biodegraded oils in the deep subsurface: part II—geological controls on subsurface biodegradation fluxes and constraints on reservoir-fluid property prediction. AAPG (Am. Assoc. Pet. Geol.) Bull. 90 (6), 921–938. https://doi.org/10.1306/01270605130.
Larter, S., Wilhelms, A., Head, I., et al., 2003. The controls on the composition of biodegraded oils in the deep subsurface—part 1: biodegradation rates in petroleum reservoirs. Org. Geochem. 34 (4), 601–613. https://doi.org/10.1016/S0146-6380(02)00240-1.
Li, N.X., Huang, H.P., Jiang, W.L., et al., 2015. Biodegradation of 25-norhopanes in a Liaohe Basin (NE China) oil reservoir. Org. Geochem. 78, 33–43. https://doi.org/10.1016/j.orggeochem.2014.10.007.
Liu, L.J., Richards, J.P., DuFrane, S.A., et al., 2016. Geochemistry, geochronology, and fluid inclusion study of the Late Cretaceous Newton epithermal gold deposit, British Columbia. Canadian J. Earth Sci. 53, 10–33. https://doi.org/10.1139/cjes-2015-0068.
Lin, H.M., Cheng, F.Q., Wang, Y.S., et al., 2017. Fluid inclusion evidence for multi-period oil charge in shahejie member 4 , Bonan subsag, Bohai Bay Basin. Oil Gas Geol. 38 (2), 209–218. https://doi.org/10.11743/ogg20170201 (in Chinese).
Lu, J.G., Ma, J., Wang, L., et al., 2016. The influence of bitumen on reservoir properties and hydrocarbon accumulation in the Santai Area of the Junggar Basin, North Western China. Petrol. Sci. Technol. 34, 464–470. https://doi.org/10.1080/10916466.2016.1145694.
Lu, J.G., Wang, L., Chen, S.J., et al., 2015. Features and origin of oil degraded gas of Santai field in Junggar Basin, NW China. Petrol. Explor. Dev. 42 (4), 466–474. https://doi.org/10.11698/PED.2015.04.03.
Moldowan, J.M., Talyzina, N.M., 1998. Biogeochemical evidence for dinoflagellate ancestors in the Early Cambrian. Science 281 (5380), 1168–1170. https://doi.org/10.1126/science.281.5380.1168.
Mu, L.X., Han, G.Q., Xu, B.J., 2009. Geology and reserve of the Orinoco heavy oil belt. Venezuela. Petrol. Expl. Develop. 36 (6), 784–789. https://doi.org/10.3321/j.issn:1000-0747.2009.06.016.
Palacas, J.G., Monopolis, D., Nicolaou, C.A., et al., 1986. Geochemical correlation of surface and subsurface oils, western Greece. Org. Geochem. 10 (1–3), 417–423. https://doi.org/10.1016/0146-6380(86)90041-0.
Pan, C.C., Tan, Y.M., Feng, J.H., et al., 2007. Mixing and biodegradation of hydrocarbons in the Daerqi oilfield, Baiyinchagan Depression, northern China. Org. Geochem. 38 (9), 1479–1500. https://doi.org/10.1016/j.orggeochem.2007.06.004.
Peters, K.E., Moldowan, J.M., McCaffrey, M.A., et al., 1996. Selective biodegradation of extended hopanes to 25-norhopanes in petroleum reservoirs. Insights from molecular mechanics. Org. Geochem. 24 (8–9), 765–783. https://doi.org/10.1016/S0146-6380(96)00086-1.
Peters, K.E., Walters, C.C., Moldowan, J.M., 2005. The biomarker guide. In: Biomarkers & Isotopes in Petroleum Systems & Earth History, , Ed2. Cambridge University Press, Cambridge, pp. 475–705.
Schaefer, R.G., Leythaeuser, D., 1980. Analysis of trace amounts of hydrocarbons (C_2-C_8) from rock and crude oil samples and its application in petroleum geochemistry. Phys. Chem. Earth 12, 149–156. https://doi.org/10.1016/0079-1946(79)90097-1.
Seifert, W.K., Moldowan, J.M., Demaison, G.J., 1984. Source correlation of biodegraded oils. Org. Geochem. 6, 633–643. https://doi.org/10.1016/0146-6380(84)90085-8.
Shalaby, M.R., Hakimi, M.H., Abdullah, W.H., 2011. Geochemical characteristics and hydrocarbon generation modeling of the Jurassic source rocks in the Shoushan Basin, north Western Desert, Egypt. Mar. Petrol. Geol. 28 (9), 1611–1624. https://doi.org/10.1016/j.marpetgeo.2011.07.003.
Shalaby, M.R., Hakimi, M.H., Abdullah, W.H., 2013. Modeling of gas generation from the alam el-bueib Formation in the shoushan basin, northern western desert of Egypt. Int. J. Earth Sci. 102 (1), 319–332. https://doi.org/10.1007/s00531-012-0793-0.
Si, S.H., Chen, H.H., Feng, Y., et al., 2013. Two sources and three charging events of hydrocarbons in Lower Cretaceous reservoirs in Shaya uplift, Tarim Basin: evidence from fluid inclusion analysis. Acta Pet. Sin. 34 (1), 12–21. https://doi.org/10.7623/syxb201301002 (in Chinese).
Sweeney, J.J., Burnham, A.K., 1990. Evaluation of a simple model of vitrinite reflectance based on chemical kinetics. AAPG (Am. Assoc. Pet. Geol.) Bull. 74 (10), 1559–1570. https://doi.org/10.1029/JB095iB11p17849.
Trendel, J.M., Guilhem, J., Crisp, P., et al., 1990. Identification of two C-10 demethylated C_{28} hopanes in biodegraded petroleum. J. Chem. Soc., Chem. Commun. 5, 424–425. https://doi.org/10.1039/C39900000424.
Volk, H., George, S.C., Middleton, H., et al., 2005. Geochemical comparison of fluid inclusion and present-day oil accumulations in the Papuan Foreland – evidence for previously unrecognised petroleum source rocks. Org. Geochem. 36, 29–51. https://doi.org/10.1016/j.orggeochem.2004.07.018.
Wang, G.L., Wang, T.G., Simoneit, B.R.T., et al., 2013. Investigation of hydrocarbon biodegradation from a downhole profile in Bohai Bay Basin: implications for the origin of 25-norhopanes. Org. Geochem. 55, 72–84. https://doi.org/10.1016/j.orggeochem.2012.11.009.
Wang, Q., Hao, F., Xu, C.G., et al., 2017. The origin and charging directions of Neogene biodegraded oils: a geochemical study of large oil fields in the middle of the Shijiutuo Uplift, Bohai Sea, China. Mar. Petrol. Geol. 88, 200–213. https://doi.org/10.1016/j.marpetgeo.2017.08.020.
Wu, K.Y., Qu, J.H., Wang, H.H., 2014. Strike-slip characteristics , forming mechanisms and controlling reservoirs of Dazhuluogou fault in Junggar Basin. J. China Univ. Petrol. (Ed. Nat. Sci.) 38, 41–47. https://doi.org/10.3969/j.issn.1673-5005.2014.05.006 (in Chinese).
Wu, K.Y., Zha, M., Liu, G.D., 2002. The unconformity surface in the Permian of Junggar Basin and the characters of oil-gas migration and accumulation. Petrol. Explor. Dev. 29 (2), 53–57. https://doi.org/10.3321/j.issn:1000-0747.2002.02.013.
Xiang, C.F., Wang, X.L., Wei, L.C., et al., 2016. Origins of the natural gas and its migration and accumulation pathways in the kelameili Gasfield. Nat. Gas Geosci. 27 (2), 268–277. https://doi.org/10.11764/j.issn.1672-1926.2016.02.0268 (in Chinese).
Yuan, F., Liao, Yh Fang, Y.X., et al., 2015. Oil-source correlation of Lower-Triassic oil seepages in Ni'erguan village, Southern Guizhou Depression, China. Acta Geochim. 35 (1), 50–63. https://doi.org/10.1007/s11631-015-0078-y.
Zhang, D.J., Huang, D.F., Li, J.C., 1988. Biodegraded sequence of Karamay oils and semi-quantitative estimation of their biodegraded degrees in Junggar Basin, China. Org. Geochem. 13 (1–3), 295–302. https://doi.org/10.1016/0146-6380(88)90048-4.
Zhang, Q., Zhu, X.M., Zhang, M.L., 2001. Seismic facies of jurassic system on east Fukang slope in Junggar Basin. J. China Univ. Petrol. (Ed. Nat. Sci.) 25 (1), 72–76. https://doi.org/10.3321/j.issn:1000-5870.2001.01.018 (in Chinese).
Zhang, S.C., Huang, H.P., 2005. Geochemistry of Palaeozoic marine petroleum from the Tarim Basin, NW China: part 1. oil family classification. Org. Geochem. 36 (8), 1204–1214. https://doi.org/10.1016/j.orggeochem.2005.01.013.
Zhang, S.C., Huang, H.P., Su, J., et al., 2014. Geochemistry of Paleozoic marine oils from the Tarim Basin, NW China. Part 4: paleobiodegradation and oil charge mixing. Org. Geochem. 67, 41–57. https://doi.org/10.1016/j.orggeochem.2013.12.008.
Zhou, S.P., Huang, H.P., Liu, Y.M., 2008. Biodegradation and origin of oil sands in the western Canada sedimentary basin. Petrol. Sci. 5 (2), 87–94. https://doi.org/10.1007/s12182-008-0015-3.
Zou, H.L., Lu, J.Q., Qiu, W., et al., 2017. The source of gas and oil in cainan oilfield jurassic layers of Junggar Basin. Petrol. Sci. Technol. 35 (19), 1873–1878. https://doi.org/10.1080/10916466.2017.1369112.